Supporting Information for

Direct Probe of Iron Vibrations Elucidates NO Activation of Heme Proteins

Weiqiao Zeng, Nathan J. Silvernail, David C. Wharton, Georgi Y. Georgiev, Bogdan M. Leu, W. Robert Scheidt, Jiyong Zhao, Wolfgang Sturhahn, E. Ercan Alp, and J. Timothy Sage

Experimental methods

Horse heart myoglobin (Sigma) was reconstituted, following a published procedure,[1] with iron protoporphyrin IX isotopically enriched in either ^{54}Fe or ^{57}Fe (Frontier Scientific). The reconstituted protein was concentrated to 10 mM in 0.1 M phosphate buffer, pH 7.0, and sodium dithionite and sodium nitrite were added to produce MbNO. Sample integrity was confirmed using visible absorption measurements prior to and resonance Raman measurements after NRVS data acquisition. Fe(TPP)(1-MeIm)(NO) was synthesized using ^{57}Fe and crystallized as described previously.[2]

NRVS data were collected at sector 3 of the Advanced Photon Source at Argonne National Laboratory, as described in detail elsewhere.[3] Briefly, a monochromator scanned the energy of the X-ray beam incident on the sample in the region of the 14.4 keV Mössbauer resonance of ^{57}Fe with 1.0 meV (= 8 cm^{-1}) resolution,[4] and emitted X-rays were detected by an avalanche photodiode. Timing circuitry excludes events coincident with the X-ray pulse, due to scattered photons, and counts events delayed in time with respect to the incident X-ray pulse, which are emitted by excited ^{57}Fe atoms. The resulting delayed count rate monitors ^{57}Fe absorption as a function of incident X-ray energy. The incident 14.4 keV X-ray flux is approximately 10^9 Hz, and comparison of initial and final scans confirms the absence of spectroscopic changes due to radiation damage.

MbNO solution and Fe(TPP)(1-MeIm)(NO) powder were loaded in polyethylene sample cells with an 80 μL volume and mounted on a helium flow cryostat. A single crystal of ^{57}Fe(TPP)(1-MeIm)(NO) was mounted on a eucentric goniometer and oriented by X-ray diffraction prior to NRVS data collection. Measurements were recorded with the X-ray beam parallel to the {001} direction of the crystal, with the crystal temperature maintained by immersion in a cold nitrogen gas stream produced by a commercial cryocooler.

Raman measurements on MbNO were performed on isotopically enriched solutions of MbNO loaded into a spinning NMR tube to minimize photolysis. Raman scattering excited by the 413.1 nm line of a krypton laser was dispersed and detected with a J-Y LabRam HR Raman microscope.

Raman data analysis

Figs. S1 and S2 show the effect of Fe and NO isotope substitution on MbNO Raman data recorded at ambient temperature. Fig. S1 is an expanded view of the same data shown in

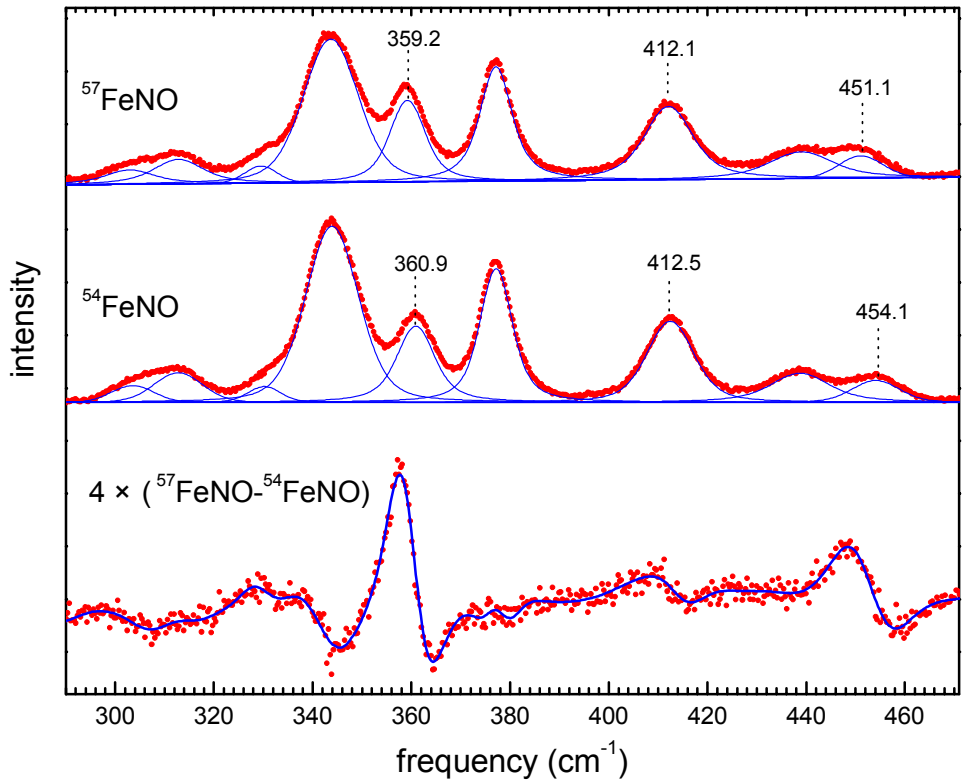

Figure S1: Fits to Raman spectra of reconstituted MbNO under 413.1 nm excitation. The upper and middle panels show results for protein reconstituted with ^{54}Fe and ^{57}Fe respectively. The lower panel is a difference spectrum. Data are represented in red and fits in blue. Data were recorded with 413.1 nm excitation on 0.34 mM solutions in 0.1 M phosphate buffer, pH 7.4.

Fig. 1. Fe isotope substitution leads to a slight change in the relative intensity, as well as the frequency, of the 360 cm^{-1} mode. Fig. S2 reveals a small shift of the 360 cm^{-1} mode on ^{14}NO$\longrightarrow$^{15}NO substitution, in addition to previously reported[5–7] band shifts near 451 cm^{-1} and 554 cm^{-1}. ^{14}NO$\longrightarrow$^{15}NO substitution alters the band shape of the feature near 550 cm^{-1}, and a ^{14}NO/^{15}NO difference spectrum indicates that at least one component of this feature undergoes a large isotopic frequency shift (Fig. S2). A minimum of three component bands were required to reproduce both sets of data near 550 cm^{-1}, and only one component exhibits a clear frequency shift. The magnitude of the frequency shift varies from 13-20 cm^{-1}, depending on the value chosen for the linewidth. Fig. S2 shows one example of such a fit. The e_N^2 value reported in Table 1 is calculated using the 16 cm^{-1} shift obtained by fitting the difference spectrum with one positive and one negative peak.

Shifts in the frequency $\bar{\nu}_\alpha$ of mode α upon changing the mass m_j of atom j were determined

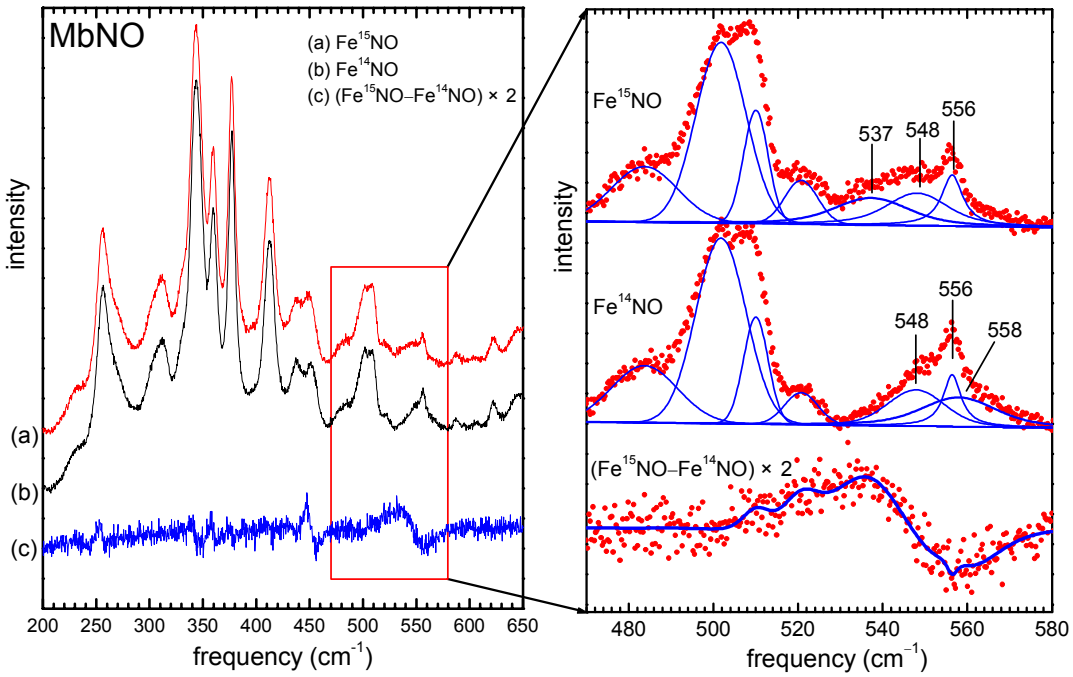

Figure S2: Fits to Raman spectra of MbNO under 413.1 nm excitation. The upper and middle panels show results for protein bound to ^{14}NO and ^{15}NO, respectively. The lower traces are difference spectra. In the right hand panel, data are represented in red and fits in blue. Data were recorded with 413.1 nm excitation on 1.0 mM solutions in 0.1 M phosphate buffer, pH 7.4, using 2.2 mW power.

by curve fitting and used to calculate an estimated mode composition factor[8]

$$e_{j\alpha}^2 = -2\frac{d(\ln \bar{\nu}_\alpha)}{d(\ln m_j)} \approx -2\frac{(\Delta\bar{\nu}_\alpha/\bar{\nu}_\alpha)}{(\Delta m_j/m_j)}.$$

This expression is valid if the normal mode eigenvector is unaltered by the mass change, and has limited validity if the isotopic frequency shift leads to vibrational mixing with other modes. The approximation is valid for small frequency changes. Frequency shifts used to calculate $e_{j\alpha}^2$ values reported in Table 1 are averaged over 2-3 independent measurements.

NRVS data analysis

The measured NRVS data are normalized according to Lipkin's sum rule[9,10] to yield a normalized excitation probability $S(\bar{\nu})$. Each vibrational mode α contributes a Stokes fundamental with area[8]

$$\phi_\alpha = (\bar{n}_\alpha + 1)\, f \frac{\bar{\nu}_R}{\bar{\nu}_\alpha} \left\langle \left(\hat{k} \cdot \vec{e}_{\mathrm{Fe}}\right)^2 \right\rangle$$

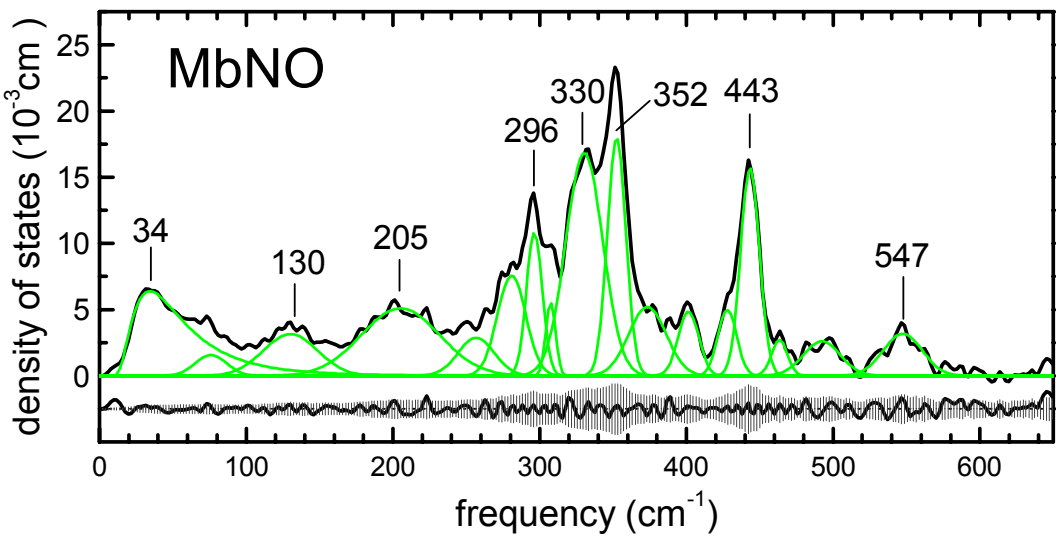

Figure S3: Fe-weighted vibrational density of states determined from NRVS measurements on MbNO. Green traces represent components of a fit, with parameters listed in the Table. Below the fitted data, the residual is compared to the calculated experimental uncertainties.

to the excitation probability at an energy $E_0 + hc\bar{\nu}_\alpha$ shifted by one vibrational quantum from (recoilless) nuclear excitation energy $E_0 = 14.4$ keV of the ^{57}Fe nucleus. Here, $\bar{n}_\alpha = [\exp(hc\bar{\nu}_\alpha/k_BT) - 1]^{-1}$ is the mean occupation number for mode α at temperature T, $hc\bar{\nu}_R = E_0^2/2Mc^2$ is the nuclear recoil energy, in terms of the nuclear mass M, and f is the recoilless fraction. The vector $\vec{e}_{j\alpha}$ is directed along the motion of atom j and its squared magnitude $e_{j\alpha}^2$ is the fraction of mode kinetic energy associated with the motion of atom j. For Fe NRVS, j =Fe and we suppress the mode index α to write $\vec{e}_{\rm Fe}$.

The angular brackets $\langle \cdots \rangle$ indicate averaging over molecular orientations with respect to the direction $\hat{k}$ of the X-ray beam. For a randomly oriented powder, $\left\langle \left(\hat{k} \cdot \vec{e}_{\rm Fe}\right)^2 \right\rangle = \frac{1}{3} e_{\rm Fe}^2$, while the angle θ between the Fe motion and the X-ray beam determines the factor $\left\langle \left(\hat{k} \cdot \vec{e}_{\rm Fe}\right)^2 \right\rangle = e_{\rm Fe}^2 \cos^2\theta$ for a perfectly oriented sample such as a single crystal. As a result, mode areas are scaled by a factor $3\cos^2\theta$ in the excitation probability measured on an oriented single crystal in comparison to the excitation probability measured on a randomly oriented polycrystalline sample of the same molecule. In particular, modes with Fe motion aligned with the X-ray beam will be selectively enhanced in the single crystal data. We have previously used single crystal NRVS measurements as an effective tool for mode assignment.[11–13]

Information on the kinetic energy distribution can be obtained conveniently from the Fe-

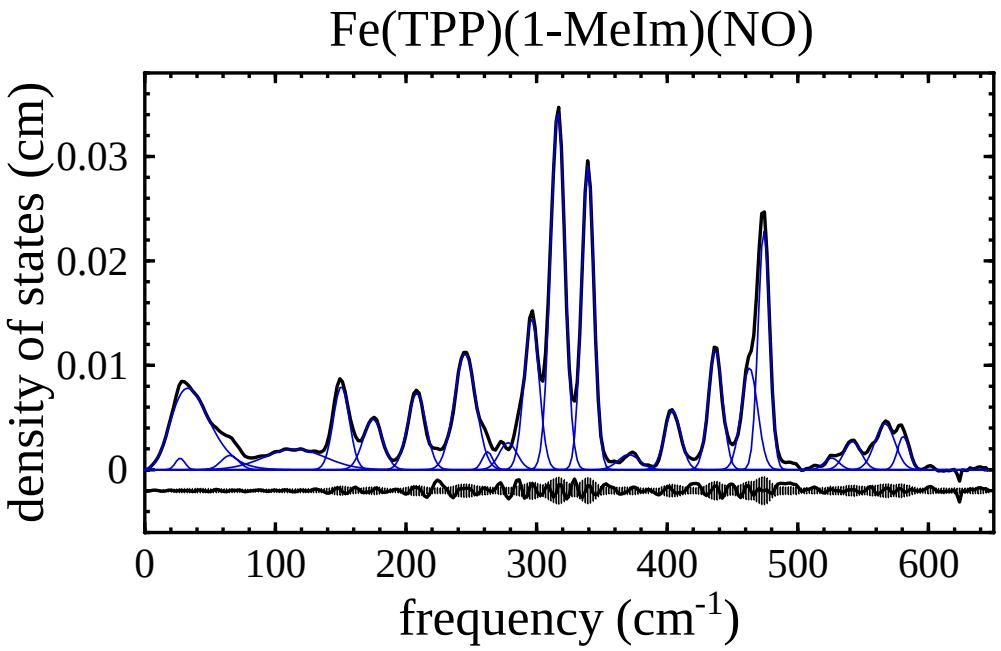

Figure S4: Fe-weighted vibrational density of states determined from NRVS measurements on Fe(TPP)(1-MeIm)(NO). Thin blue traces represent components of a fit, with parameters listed in the Table. Below the fitted data, the residual is compared to the calculated experimental uncertainties.

weighted vibrational density of states (VDOS) $D(\bar{\nu})$, extracted using the program PHOENIX.[14] In the VDOS representation of the data, each vibrational mode contributes an area e^2_{Fe} equal to the fraction of mode energy associated with motion of the Fe atom. Tables S1 and S2 list this area, together with the mode frequency and full width at half maximum (FWHM), for MbNO and Fe(TPP)(1-MeIm)(NO), respectively. Figs. S3 and S4 display the components of the fit to the experimental VDOS used to obtain these values.

Table S1: Fit parameters describing the Fe-weighted vibrational density of states for MbNO. All components of the fit function are Gaussians, with the exception of a log-normal curve at 34.3 cm^{-1}.

frequency (cm^{-1})	e^2_{Fe}	FWHM (cm^{-1})
34.3	0.349	45.6 (2.18[a])
75.9	0.042	25.4
130.2	0.146	43.5
205.1	0.340	62.8
256.7	0.089	29.1
280.9	0.184	22.8
296.3	0.146	12.7
307.4	0.046	7.8
330.5	0.532	29.7
352.5	0.284	14.8
373.5	0.166	30.0
401.4	0.085	16.5
427.9	0.080	15.0
443.4	0.252	15.1
463.4	0.037	12.8
492.3	0.083	29.7
547.4	0.106	31.2

*a.*Dimensionless asymmetry parameter.

Table S2: Fit parameters describing the Fe-weighted vibrational density of states for Fe(TPP)(1-MeIm)(NO). All components of the fit function are Gaussians, with the exception of a log-normal curve at 32.9 cm^{-1}.

frequency (cm^{-1})	e^2_{Fe}	FWHM (cm^{-1})
27.1	.010	8.5
32.9	.293	34.7 (1.31[a])
65.2	.023	15.9
114.8	.116	55.0
150.5	.122	14.4
174.7	.090	17.4
208.3	.129	16.6
245.2	.231	19.5
262.5	.017	9.4
278.2	.044	16.0
296.2	.207	13.4
316.2	.478	13.1
339.1	.348	11.2
370.6	.030	19.4
404.2	.088	14.5
436.9	.156	12.8
463.0	.153	14.7
474.0	.251	10.3
525.9	.016	13.5
542.0	.045	15.5
566.7	.085	17.9
580.8	.035	10.3

*a.*Dimensionless asymmetry parameter.

References

1. Teale, F. W. J. *Biochim. Biophys. Acta* **1959,** *35,* 543.
2. Wyllie, G. R. A.; Schulz, C. E.; Scheidt, W. R. *Inorg. Chem.* **2003,** *42,* 5722-5734.
3. Sturhahn, W. *J. Phys.: Condensed Matter* **2004,** *16,* S497-S530.
4. Toellner, T. S. *Hyp. Int.* **2000,** *125,* 3-28.
5. Benko, B.; Yu, N. T. *Proc. Natl. Acad. Sci. USA* **1983,** *80,* 7042-7046.
6. Hu, S.; Kincaid, J. *J. Am. Chem. Soc.* **1991,** *113,* 9760-9766.
7. Tomita, T.; Hirota, S.; Ogura, T.; Olson, J. S.; Kitagawa, T. *J. Phys. Chem. B* **1999,** *103,* 7044-7054.
8. Sage, J. T.; Paxson, C.; Wyllie, G. R. A.; Sturhahn, W.; Durbin, S. M.; Champion, P. M.; Alp, E. E.; Scheidt, W. R. *J. Phys.: Condens. Matter* **2001,** *13,* 7707-7722.
9. Lipkin, H. J. *Ann Phys (NY)* **1962,** *18,* 182.
10. Sturhahn, W.; Toellner, T. S.; Alp, E. E.; Zhang, X.; Ando, M.; Yoda, Y.; Kikuta, S.; Seto, M.; Kimball, C. W.; Dabrowski, B. *Phys. Rev. Lett.* **1995,** *74,* 3832-3835.
11. Rai, B. K.; Durbin, S. M.; Prohofsky, E. W.; Sage, J. T.; Wyllie, G. R. A.; Scheidt, W. R.; Sturhahn, W.; Alp, E. E. *Biophys. J.* **2002,** *82,* 2951-2963.
12. Rai, B. K.; Durbin, S. M.; Prohofsky, E. W.; Sage, J. T.; Ellison, M. K.; Scheidt, W. R.; Sturhahn, W.; Alp, E. E. *Phys. Rev. E* **2002,** *66,* 051904.
13. Leu, B. M.; Zgierski, M. Z.; Wyllie, G. R. A.; Scheidt, W. R.; Sturhahn, W.; Alp, E. E.; Durbin, S. M.; Sage, J. T. *J. Am. Chem. Soc.* **2004,** *126,* 4211-4227.
14. Sturhahn, W. *Hyp. Int.* **2000,** *125,* 149-172.